Development of Mixed Pitch Grating for the Optical Addressing of Trapped Sr + Ion with Data Analysis Techniques

Yu Dian Lim, Peng Zhao, Liangxing Hu, Luca Guidoni, Jean-Pierre Likforman, Chuan Seng Tan

Development of Mixed Pitch Grating for the Optical Addressing of Trapped Sr^+ Ion with Data Analysis Techniques

YU DIAN LIM,[1,*] PENG ZHAO,[1,2] LIANGXING HU,[1] LUCA GUIDONI,[3] JEAN-PIERRE LIKFORMAN,[3] AND CHUAN SENG TAN[1,2,*]

[1] *School of Electrical and Electronics Engineering, Nanyang Technological University, 639798, Singapore*
[2] *Institute of Microelectronics, Agency for Science, Technology and Research (A*STAR), 117685, Singapore*
[3] *Laboratoire Matériaux et Phénomènes Quantiques (MPQ), Université de Paris, F-75205 Paris, France*
*yudian.lim@ntu.edu.sg
*tancs@ntu.edu.sg

Abstract: Mixed pitch gratings are developed for the optical addressing of trapped $^{88}Sr^+$ ion by means of simulation and experimental-measurement approaches. Meanwhile, Python-based data analysis techniques were developed to analyze simulated and measured beam profiles. A fixed pitch grating with a pitch of 1.2 µm was used as a reference, and a mixed pitch grating with pitches of 1.1/1.2 µm of various ratios are investigated. The Python-based data analysis codes demonstrates highly-automated capability in processing both simulated and measured beam profile data to compute key parameters, including beam waist and Gaussian fitting. Mixed pitch grating delivers light beam with smaller beam waist (17.4 µm) compared to the fixed pitch grating (26.4 µm), exhibiting ~34% beam waist reduction.

1. Introduction

Trapped ion quantum computer has attracted much attention due to its high fidelity [1,2] and low error among identical trapped ion qubits [3]. Fundamentally, the usage of trapped ion quantum computer involves optical addressing of trapped ion with laser light of specific wavelengths to perform various computing tasks: including <1>/<0> transition, ion-cooling, clear-out etc. [4] For optical addressing, silicon photonics components (waveguide, gratings) can be integrated into the surface electrode ion trap to miniaturize the formfactor of the trapped ion quantum computer, as reported by several studies [3,5–7]. The illustration of optical addressing by integrated grating is illustrated in Fig. 1(a).

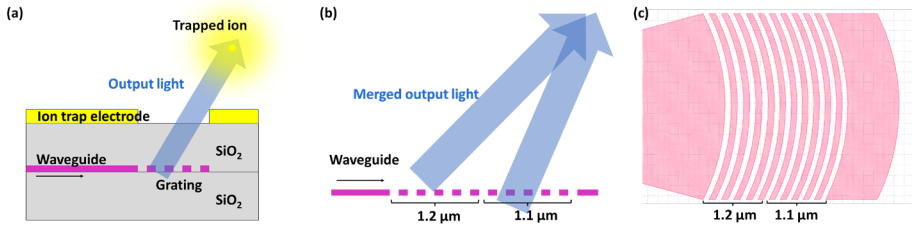

Fig. 1. (a) Illustration of optical addressing of trapped ion using integrated grating, (b) illustration of light focusing using mixed pitch grating, (c) typical GDS layout of mixed-pitch grating

To ensure accurate optical addressing on individual trapped ions using integrated grating structure, the beam coupled out from the grating structure should be focused. Various

techniques have been reported to enhance the focusing of light beam coupled out from the grating. For instance, apodised grating structure is reported to enhance the focusing of the grating to improve its corresponding coupling efficiency [8]. At the same time, Kim et al. reported the usage of compact planar photonic structure consists of two output gratings to form a well-collimated near surface-normal Gaussian beam [9]. Meanwhile, Becker et al. reported out-of-plane focusing grating coupler with dual waveguide inputs towards the same grating structure, and enhance the focusing my introducing a phase-change to one of the waveguides [10]. Besides, Zhong et al. introduced tapered structure grating to suppress the back reflection of the curved grating, and enhance its associated focusing and the coupling efficiency [11]. Despite the on-going efforts in the engineering of grating structure for focused output beams, the state-of-the-art designs often involves customized design and fabrication steps. For instance, apodised grating requires high-resolution photolithography and etching techniques. This ensures the continuity of increasing grating pitch to fulfill the apodization condition. These limitations hinder the commercialization and mass production of grating-integrated ion traps, or other devices involving integrated gratings.

In this study, a simple miedx pitch grating is developed to improve the focusing of light from grating structure. As the angle of the output light increases with increasing grating pitch [12,13], mixing two similar pitches in a single grating can expect a focused beam by merging light coupled out from different pitches, as illustrated in Fig. 1(b). A typical grating design is illustrated in Fig. 1(c). On top of that, this study also introduces a Python-based analysis technique to analyze the beam characteristics at various heights (from the grating), including Gaussian fitting, beam energy, beam waist, etc.

2. Design and Simulation

In this study, 1092 nm wavelength is selected for the grating design as 1092 nm is associated to the clear-out function of the trapped $^{88}Sr^{+}$ ion quantum computer [14,15]. To design grating structure for the optical addressing of trapped ion qubits, several conditions should be set. First, the grating should be placed as far as possible from the trapped ion position, while the output light hitting the trapped ion. As shown in Fig. 1(a), openings are required on the ion trap electrode to facilitate the optical addressing [16]. These openings will result in formation of stray electric field along the edges of the opening, which affect the ion-trapping performance of the ion trap [17,18]. Thus, grating structure with large angle of inclination from the vertical is preferred. Second, the height where the ion(s) are trapped can be adjusted by the dimension of the ion trap. Typically, the ions are trapped at 20, 40 or 80 μm from the electrode surface as reported in our earlier studies [18,19]. Finally, the angle of the output light, θ, can be expressed as:

$$\Lambda=\frac{m\lambda}{N-n_1 \sin\theta} \quad (1)$$

where Λ, m. λ, N, and n_1 are the grating pitch, mode, wavelength, effective index of the grating, and index of the fiber, respectively. From Eq. (1), it can be deduced that the angle, θ, increases with increasing grating pitch, Λ. Third, the distance between trapped ions ranges from 10 to 20 μm, depending on the design of the ion trap and the electric signals introduced to the ion trap [20].

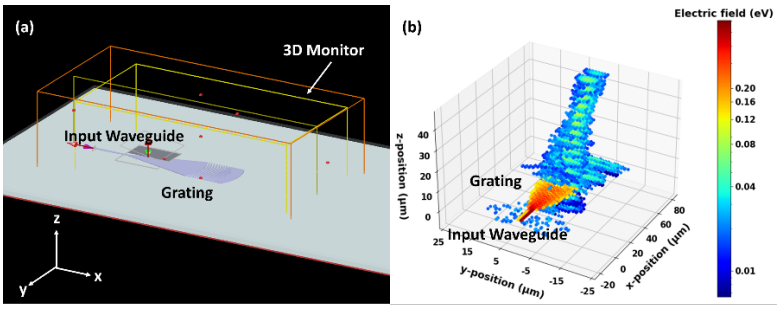

Fig. 2. (a) Simulation model of the Finite-Difference Time-Domain (FDTD) simulation, (b) 3D E-field distribution plot from the 3D monitor (1.2 μm pitch grating)

To enhance the focusing of light coupled out from grating, mixed-pitch gratings with 1.1 and 1.2 μm grating pitches are investigated. In determining the simulated beam characteristics, Finite-Difference Time-Domain (FDTD) simulation is carried for SiN waveguide and gratings with 3 μm buried oxide layer (BOX) and 2 μm top oxide layer (TOX). Fig. 2(a) shows the simulation model used in this study. In a typical simulation, light with 1092 nm wavelength will propagate through the input waveguide and coupled out from the grating. A three-dimensional (3D) monitor is used to capture the electric field energy (E-field) in eV of the coupled light. The obtained 3D distribution will be saved into a 1950×975×375 3D array for further data analyses using Python-based tool. The material of the grating is SiN, where the duty cycle, SiN thickness, etch depth, and radius of curvature of the grating are fixed at 0.5, 0.4 μm, 0.4 μm, and 20 μm, respectively. A typical E-field distribution plot is shown in Fig. 2(b). From Fig. 2(b), it can be seen that the output light beam propagates towards x-z plane with inclined angle with respect to the vertical (z-axis).

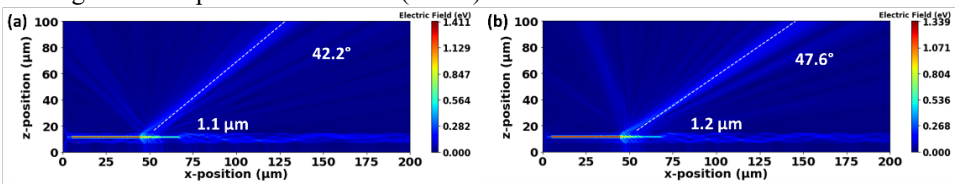

Fig. 3. E-field plot along x-z plane from grating with (a) pitch = 1.1 μm, (b) pitch = 1.2 μm

To determine the fundamental optical characteristics of light beam coupled out from the SiN grating, several simulations and data analyses are first carried out. The E-field simulation along x-z plane for gratings with pitch size of 1.1 and 1.2 μm is carried out. The obtained E-field distribution is then imported into a DataFrame in Python. The maximum E-field value at each row (along x-axis) of the DataFrame is then obtained. The linear plot, including the slope values and the corresponding θ values are obtained with linear-fitting using scipy package. The snippet of the code to carry out these is described in Fig. S1 in the supplementary material. The full code to carry out these is presented in ref. [21]. From Fig. 3, it can be observed that 1.2 μm pitch grating shows a larger θ = 47.6° value compared to its 1.1 μm counterpart (θ = 42.2°). As illustrated in Fig. 1(b), 1.1 and 1.2 μm pitches can be mixed in a grating for merged beam.

To further investigate the beam characteristics, the beam waists (along x- and y-axis) at various heights (along z-axis) are computed. The beam waists are defined as the width of the E-field distribution along x- and y-axis at 0.135 (equivalent to $1/e^2$) of the peak. As mentioned earlier, the obtained 3D E-field distribution will be saved into a 1950(x) ×975(y) ×375(z) array for further Python-based data analyses. The E-field distribution in x-y plane will first be extracted as two-dimensional (2D) DataFrame, layer-by-layer along z-axis. After that, the beam waists (along x- and y-axis) at each layer (or height along z-axis) will be computed using scipy package. Fig. 4(a) shows the typical scenario of finding beam waists. As shown, multiple peaks

often present in a single plot (the Gaussian fitting illustrated in Fig. 4(b) will be discussed later). Thus, only the beam waist associated to the highest peak will be taken into consideration. The full code in computing the beam waists and finding the maximum E-field at each x-y plane is shown in ref. [22], while the snippet of the code is described in Fig. S2 of the supplementary material. The obtained beam waists are then plotted in Fig. 5(a) and (b). The full Python code used to plot Fig. 5(a) and (b) is in ref. [23].

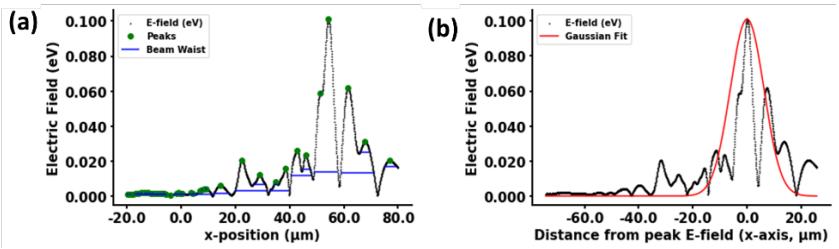

Fig. 4. Typical scenario of: (a) finding the peaks and the associated beam waists along x-axis, (b) Gaussian fitting of E-field along x-axis

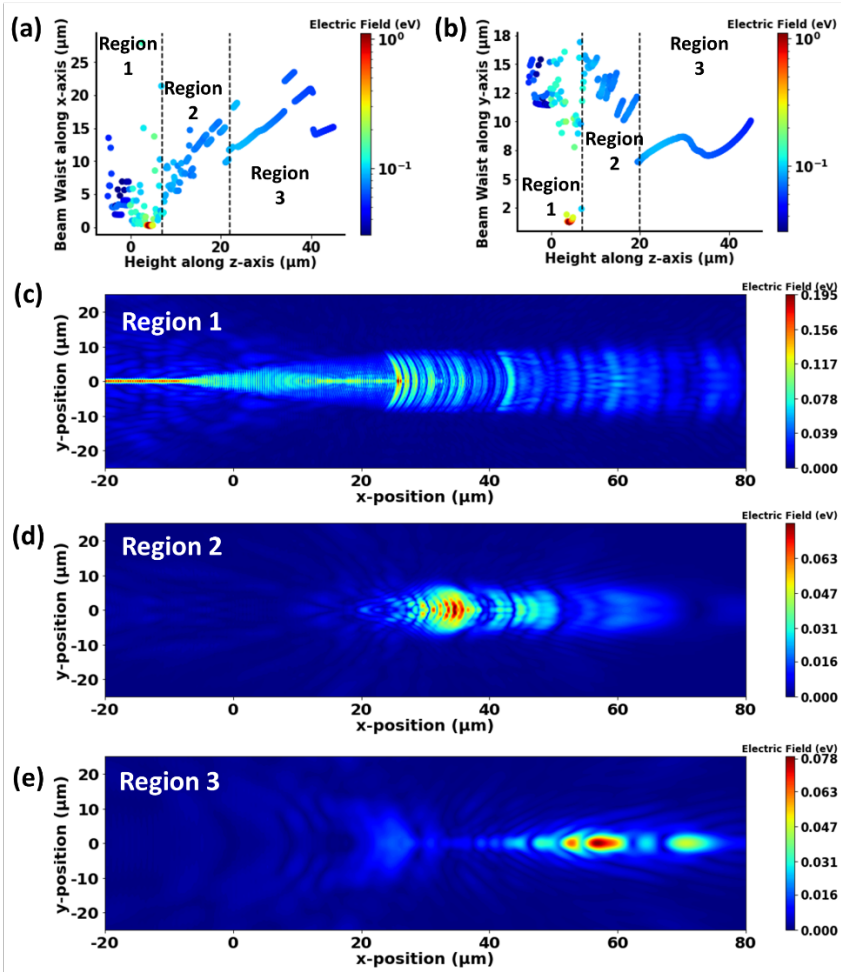

Fig. 5. Beam waist and E-field at various heights (z-axis): (a) along x-axis, (b) along y-axis; beam shape at x-y plane in: (c) Region 1, (d) Region 2, (e) Region 3

The beam waists (along x- and y-axis) at different heights can be segmentized into Region 1, Region 2, and Region 3. Region 1 represents the height range from the BOX layer to TOX layer, including the 0.4 μm SiN grating. Thus, Region 1 has high E-field, and the E-field distribution along the waveguide and the grating is visible, as shown in Fig. 5(c). At Region 2, the light was propagated to free space, where the beam shape started to form. However, the fringes resulted from the grating structure is still visible, as shown in Fig. 5(d). The changes in beam waists along z-axis are scattered with no regular pattern, as shown in Fig. 5(a) and (b). This region can be deduced as reactive near distance region where the E-Field and magnetic field (H-Field) are 90 degrees out of phase with each other and are therefore reactive. The reactive field region ranges between the grating to $0.62(\sqrt{\frac{D^3}{\lambda}})$ above the grating, where D is the maximum linear dimension of the grating and λ is the wavelength [24]. As the grating used in this study has a D value of ~10 μm, the calculated value for $0.62(\sqrt{\frac{D^3}{\lambda}})$ is ~18.76 μm, which aligns with Fig. 5(a) where the reactive near field region ends at height = ~ 22 μm (grating is located at height = ~4 μm). At Region 3, Gaussian-like beams started to form with multi-mode presence (Fig. 5(e)). At the same time, the changes of beam waist along z-axis are somehow regular, as shown in Fig. 5(a) and (b). The beam waists at near reactive field (Region 2) region are irregular, which possesses significant challenges in performing systematic investigation. Moreover, the typical ion-trapping height is ~20, 40 or 80 μm above the ion trap electrode, as mentioned in the beginning of the section. ~20 μm above the ion trap electrode translates to ~23 μm in the context of Fig. 5(a) and (b), which falls in Region 3. Thus, this study will focus on investigating the beam waists in Region 3.

Table 1. Sample Labeling and Description

Sample Labeling	Sample Description
10(1.2 μm)	Fixed 1.2 μm pitch (no pitch mixing)
8(1.2 μm) : 2(1.1 μm)	80% of 1.2 μm pitch, 20% of 1.1 μm pitch
6(1.2 μm) : 4(1.1 μm)	60% of 1.2 μm pitch, 40% of 1.1 μm pitch
5(1.2 μm) : 5(1.1 μm)	50% of 1.2 μm pitch, 50% of 1.1 μm pitch
4(1.2 μm) : 6(1.1 μm)	40% of 1.2 μm pitch, 60% of 1.1 μm pitch
2(1.2 μm) : 8(1.1 μm)	20% of 1.2 μm pitch, 80% of 1.1 μm pitch

To develop grating with optimized focusing, gratings with various 1.2μm/1.1 μm ratios are investigated. Table 1 shows the sample labeling investigated in this study. For the sake of simplicity, sample "8(1.2 μm) : 2(1.1 μm)", "6(1.2 μm) : 4(1.1 μm)", "5(1.2 μm) : 5(1.1 μm)" … will be simplified as "8(1.2 μm)", "6(1.2 μm)", "4(1.2 μm)" …, in the text body.

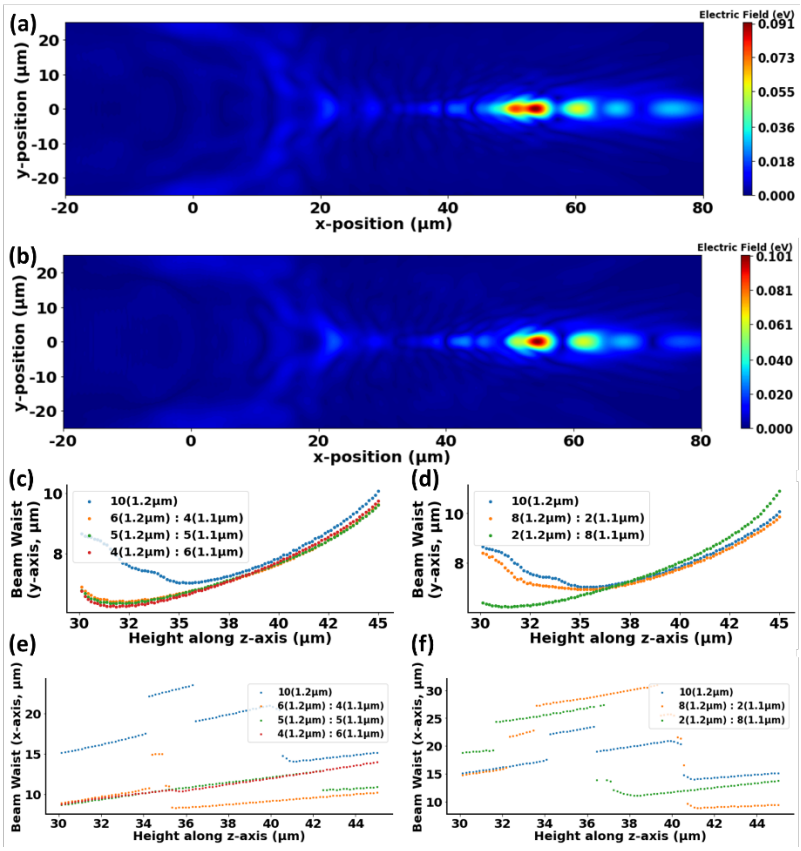

Fig. 6. (a) E-field distribution at x-y plane for (a): 8(1.2 µm) : 2(1.1 µm) grating, (b) 6(1.2 µm) : 4(1.1 µm) grating grating; (c) and (d): beam waist along y-axis, (e) and (f): beam waist along x-axis

Fig. 6 shows the beam waist of the light coupled out from pure 1.2 µm pitch grating and 1.2 µm/1.1 µm mixed pitch grating. From Fig. 6(a), it can be observed that 8(1.2µm) grating shows larger beam waist along x-axis compare to 10(1.2µm) grating shown in Fig. 5(e). As compared to 8(1.2µm) grating, 6(1.2µm) grating has smaller beam waist along x-axis compare to 8(1.2µm) and 10(1.2µm) grating with higher E-field value, which implies that 6(1.2µm) mixed pitch grating delivered more focused light beam compared to fixed pitch grating. To avoid confusion, the investigated mixed-pitch gratings are plotted separately, as shown in Fig. 6(c) and (d), Fig. 6(e) and (f). From Fig. 6(c) and (d), the beam waist along y-axis do not show significant difference between fixed pitch grating and mixed pitch gratings. As the beam waist along y-axis mainly depend on the taper shape and the radius of curvature [25], mixing the pitch in the grating shall not have direct influence towards the beam waist along y-axis. Whereas for beam waist along x-axis, it is observed that 6(1.2µm), 5(1.2µm), and 4(1.2µm) mixed pitch gratings show lower beam waists (Fig. 6(e)). For instance, the beam waist reduces from 17 µm to 10 µm at 32 µm height. This indicates that the light from 1.2 µm and 1.1 µm pitches to form a focused, collimated beam. On the other hand, the 8(1.2µm) and 2(1.2µm) mixed pitch gratings has higher beam waist than fixed pitch grating. For instance, the beam waist of mixed pitch gratings is larger (22 - 25 µm) than fixed pitch grating (17 µm) at 32 µm height. This can be attributed to the scattering of light, due to the interference within mixed pitch gratings with imbalance mixture ratio.

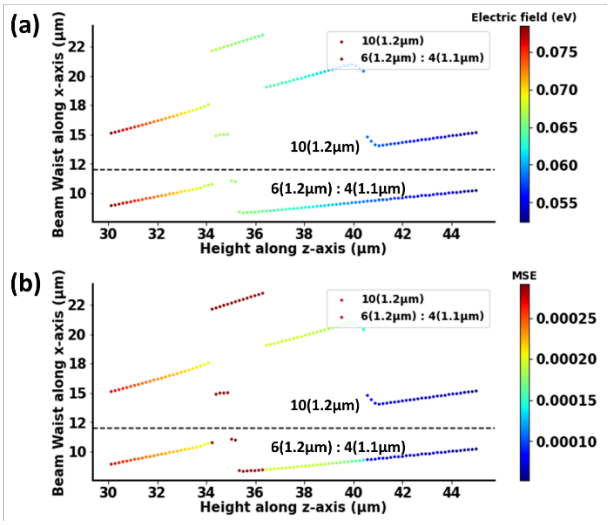

Fig. 7. Comparison between fixed pitch and mixed pitch gratings: (a) Peak E-field, (b) mean squared error of Gaussian fit.

To further investigate the beam characteristics of mixed pitch and fixed pitch grating, the maximum E-field at various heights is obtained and plotted in Fig. 7(a). Taking 6(1.2 μm) grating as a typical example, it is observed that mixed pitch gratings do not show significant difference in E-field changes along z-axis as compared to mixed pitch gratings. Thus, it can be deduced that the implementation of mixed pitch gratings merely enhances the focusing of light beam coupled out from the grating, without much enhancement on the output coupling energy. At the same time, Gaussian beam fitting of the E-field is also attempted at various heights, along x-axis. The Gaussian beam distribution can be expressed as:

$$E_s = E_0 . exp\left(-\frac{r^2}{{\omega_0}^2}\right) \quad (2)$$

where E_0 is the peak E-field at the centre of the beam, r is the distance from the centre of the beam, ω_0 is the beam waist. A typical Gaussian-fitting is shown in Fig. 4(b). From Fig. 4(b), it can be observed that the Gaussian plot does not fit well with the single, highest peak of the E-field distribution [26]. To determine the Gaussian fitting of the light beam at various heights, the mean squared error (MSE) of the Gaussian fitting is computed at various heights using Python-based computation, where the outcomes are plotted in Fig. 7(b). The full Python code is shown in ref. [21], while the snippet of the code is described in Fig. S3. From Fig. 7(b), the MSE reduces at higher z-position, indicating that the beam exhibits more Gaussian-like characteristics as the beam propagates towards z-axis. Nevertheless, the MSE values for both fixed pitch and mixed pitch gratings are similar, indicating that the implementation of pitch mixing does not incur significant changes on the E-field distribution within the light beam. Thus, in the next section where experimental data are presented, the study will focus on the changes in beam waist from pitch-mixing.

3. Experimental Details

The SiN gratings used in the simulations discussed the previous section were fabricated using a multi-project wafer (MPW) service. This fabricated process involved depositing a buried-oxide-layer (BOX) with a thickness of 3 μm onto a 200 mm silicon wafer surface, followed by the deposition of 0.4 μm thick SiN. The SiN layer was then subjected to dry etching to create etch-through grating structures. A layer of 3 μm thick top-oxide-layer (TOX) was then deposited on the grating structure. The test structure used for the SiN-based grating is illustrated

in Fig. 8(a). This structure uses an input grating to couple 1092 nm light into the waveguide, which is then split into multiple channels using a multi-mode interferometer (MMI) and directed to respective gratings. The reference gratings (ref. grating) is identical as input grating, with 0.8 µm pitch and 0.5 duty cycle with optimized coupling efficiency for 1092 nm wavelength. As the reference grating is expected to deliver brightest beam profile, it is used to identify the orientation of the light beams during beam profiling.

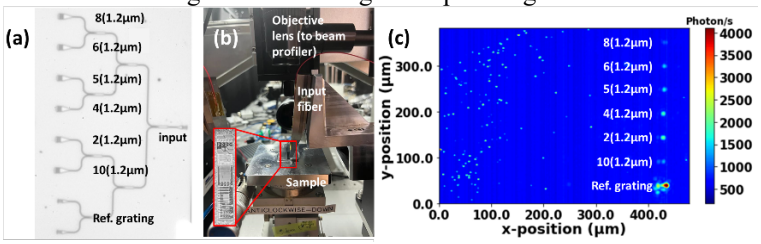

Fig. 8. (a) Test structure used in this study, (b) beam profiling system (inset: photograph of the sample), (c) beam profile obtained from the sample

Fig. 8(b) shows the beam profiling measurement system. During a typical measurement, the input fiber is directed onto the sample chip to couple 1092 nm laser light (Innolume DFB laser) into the test structure via the input grating. The input fiber is inclined at $\theta = 13°$ from the vertical computed by Eq. (1). The 1092 nm light is then coupled into the input grating and split equally to 8 different waveguides through the optimized multi-mode interferometer (MMI). The output light from the gratings (mixed pitch, fixed pitch, ref. grating) are then captured by a series of objective lenses and transmitted to the infra-red beam profiler (Ophir XC-130). Once initial beam profiles are visible from the beam profiler, the height of the beam profiler is adjusted manually till a sharpest-possible image is obtained, as shown in Fig. 8(c).

The obtained beam profile data (from Fig. 8(c)) in photon count per second (cnt/s) is then saved into a 2D DataFrame. The beam profiles from their respective gratings (labeled in Fig. 8(c)) are then diced into individual DataFrame and analyzed with Python-based data analysis tools.

4. Results and Discussion

Fig. 9 shows the beam profiles of light coupled out from 10(1.2µm), 4(1.2µm), and 8(1.2µm) gratings. In Fig. 9(a), two beams along x-position are observed as 1092 nm light coupled out from 10(1.2µm) grating, due to the presence of multi-mode beams. The obtained multi-mode beam profile is similar to the E-field distribution in Fig. 5(e). For beam profile from 4(1.2µm) grating shown in Fig. 9(b), the beam profile is more focused, similar to the E-field distribution in Fig. 6(b). For beam profile from 8(1.2µm) grating shown in Fig. 9(c), undesired light-interaction between light from 1.1 and 1.2 µm pitches hinders the beam collimation of 1092 nm light. This result in formation of irregular, asymmetrical beam shape, with significantly lower intensity (cnt/s).

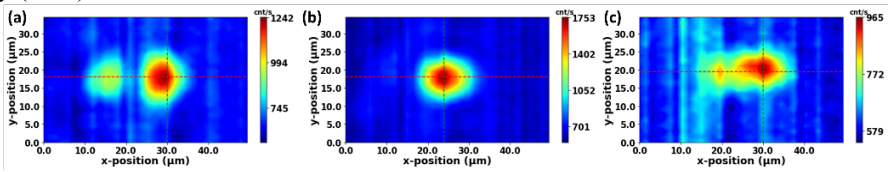

Fig. 9. Beam profile of light coupled out from the following gratings: (a) 10(1.2µm), (b) 4(1.2µm), (c) 8(1.2µm)

The dotted lines in Fig. 9 represents the cut-off lines along x- and y-axis where the highest cnt/s value within the DataFrame (higher cnt/s value) is located. The cut-off lines are computed and plotted using automated Python-based data analysis technique, where the full code is shown in ref. [27] and the snippet of the code is described in Fig. S4 in the supplementary material.

From Fig. 9, it can be observed that 10(1.2µm), 4(1.2µm), and 8(1.2µm) gratings do not show much differences in beam waists along y-axis. This agrees well with Fig. 6, where the merging of light beam from different pitches is more significant along x-axis as compared to y-axis. Nevertheless, the photon count (cnt/s) along x- and y-axis (horizontal and vertical dotted lines in Fig. 9 are plotted in Fig. 10. In Fig. 10(b), the beam waist along y-axis does not exhibit significant changes as compared to x-axis in Fig. 10(a). By using the Python-based data analysis techniques with scipy package, the beam waist along y-axis is ~16 µm for light beam from 10(1.2µm) fixed pitch grating, which reduces slightly to 14-15 µm for mixed pitch gratings (not shown). The slight reduction of beam waist can be attributed to slight focusing of light beam along y-axis, due to the curved-shaped of the grating structure. To further investigate the beam waist along x-axis, Python-based data analysis technique is used to locate the peaks present in the photon count plots in Fig. 10(a), where the corresponding beam waists and full width half maximum (FWHM) of each peak are computed. The full code is presented in ref. [28].

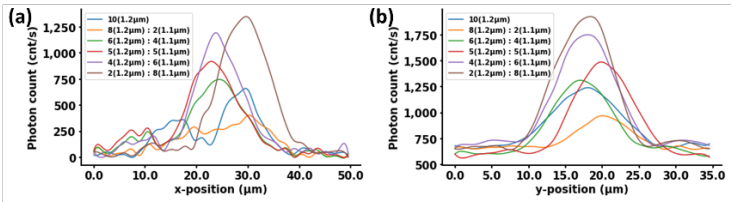

Fig. 10. Photon count plot along (a) x-axis, (b) y-axis

Fig. 11 shows the photon count plot along x-axis of light coupled out from fixed pitch (10(1.2µm)) and mixed pitch (4(1.2µm) and 8(1.2µm)) gratings. From Fig. 11, it can be observed that multiple peaks are identified by scipy package in Python. Two distinctive peaks are present in Fig. 11(a), attributing to the multi-mode beams observed in Fig. 9(a) and Fig. 5(e). As the beam waist is computed by taking the peak at $1/e^2$ of the peak value, scipy computation considered the two peaks coincided, resulting in large beam waist. For mixed pitch 8(1.2µm) grating, the beam waist is larger than fixed pitch 10(1.2µm) grating with lower cnt/s. This can be attribute to undesired interference between disproportional mixture of 1.1 and 1.2 µm pitches, which is reflected in both simulated (Fig. 6(f)) and experimental (Fig. 9(c)) outcomes. As compared to the abovementioned gratings, mixed pitch 4(1.2µm) grating delivers more focused light beam, with higher cnt/s values as compared to 10(1.2µm) and 8(1.2µm) counterparts.

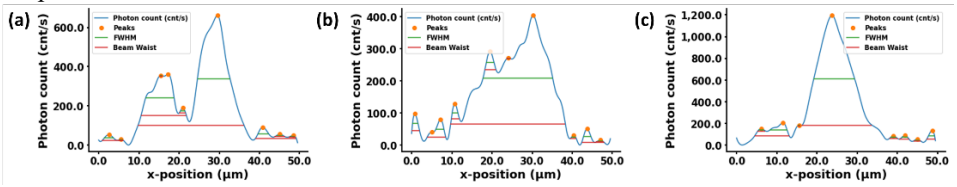

Fig. 11. Photon count, peaks, beam waist and FWHM of light coupled out from the following gratings: (a) 10(1.2µm), (b) 8(1.2µm), (c) 4(1.2µm)

The simulated and measured beam waists with their respective peak E-field (simulated) and photon count (measured) is compiled in Fig. 12. The simulated beam waist presented in Fig. 12 is taken near the surface of the TOX. Overall, both simulated beam waist and measured beam waist shows similar trend. For the measured data, beam waist (along x-axis) increases significantly from 10(1.2µm) grating to 8(1.2µm), from 26.4 to 28.6 µm due to the undesired interference between disproportional mixture of 1.1 and 1.2 µm pitches. After that, the beam waist gradually reduces from 8(1.2µm) to 4(1.2µm), reaching the lowest point at 4(1.2µm) with 17.4 µm, showing ~34% in beam waist reduction. The beam waist increases slightly from 4(1.2µm) to 2(1.2µm) to 18.5 µm. For photon count (cnt/s), the measured beam profile from

10(1.2µm) grating has peak photon count of 1242 cnt/s, which reduces to 965 cnt/s as it shifted to 8(1.2µm). 4(1.2µm) and 6(1.2µm) gratings show similar peak photon count of 1307 and 1331 cnt/s. Meanwhile, light from 5(1.2µm) grating has lower peak photon count of 1008 cnt/s. The light from 2(1.2µm) grating exhibits highest peak photon count of 1924 cnt/s.

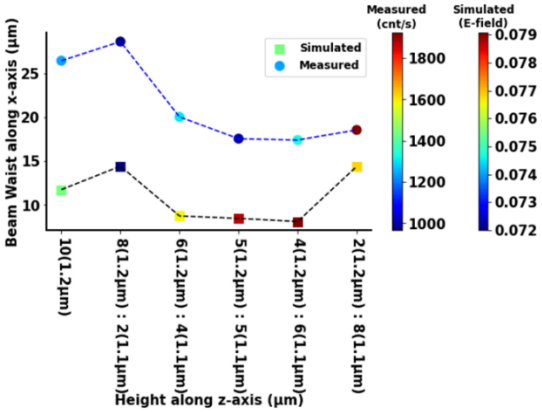

Fig. 12. Comparison between simulated and measured beam waist

Generally, the simulated properties of light beam from fixed pitch and mixed pitch gratings aligns with the measured beam profile. The simulated beam waist from 10(1.2µm) grating is 11.7 µm, which increases to 14.4 µm when 8(1.2µm) grating is used. After that, the beam waist reduced to 8.1 – 8.7 µm for 6(1.2µm), 5(1.2µm), and 4(1.2µm) gratings. The beam waist rebound to 14.4 µm for 2(1.2µm) grating, with higher peak E-field as compared to 10(1.2µm) grating. Both simulated and measured beams exhibit reduction of peak E-field/photon count when shifting from 10(1.2µm) to 8(1.2µm) grating, and increase of peak E-field/photon count when shifting from 4(1.2µm) to 2(1.2µm) grating. The reduction can be attributed to undesired interference between disproportional mixture of 1.1 and 1.2 µm pitches as mentioned earlier. The increase in peak E-field/photon count can be attribute to the presence grating structure with more 1.1 µm pitch, which exhibits higher output coupling efficiency, as implied in Fig. 3.

Despite simulated outcomes align well with experimentally-measured result in general, there are still some discrepancies between simulated and measured results. The changes in peak E-field/photon count as we shift from 6(1.2µm) grating to 4(1.2µm) exhibits some discrepancy between simulated E-field and measured photon count. This can be due to possible manufacturing error in the grating, where various factors, including sidewall roughness, inaccuracy in photolithography and dry etching process, and unevenness in the TOX oxide layer can result in lower output coupling efficiency. This may result in lower-than-expected energy in the output beams from the grating. At the same time, the simulated beam waists are generally smaller than the measured beam waist. This can be due to the imperfect focusing of the beam profile. As mentioned in Section 3, the height of the beam profiler is adjusted manually till a sharpest-possible image is obtained during a typical measurement. Manual adjustment may result in imperfect focusing, resulting in the formation of large beam waists. At the same time, the resolution of the beam profiler may be limited, which is not able to capture the light beam as sharply as simulation results. Nevertheless, this study demonstrates the implementation of mixed pitch grating to reduce the beam waist of the light from grating, where the reduction is observed in both simulated and measured data. Mixture of 1.1/1.2 µm pitches with various ratio are investigated to provide several choices of gratings for the optical addressing of trapped $^{88}Sr^{+}$ ions, depending on the ion trapping height, distance between trapped ions, etc. Finally, the Python-based data analysis demonstration introduced an automated solution to analyze the beam profiles for both simulated and measured data. Combining these results, the outcomes obtained in this study can provide a more automated, simple solution to the focusing of grating for the optical addressing of $^{88}Sr^{+}$ ions using 1092 nm laser light.

5. Conclusion

In this study, mixed pitch grating is designed and developed for the optical addressing of trapped $^{88}Sr^{+}$ ion. Laser light of 1092 nm wavelength is selected as it corresponds to the clear-out function in trapped $^{88}Sr^{+}$ ion. At the same time, Python-based data analysis techniques are developed to automate large-scale analysis on both simulated and measured beam profiles. Fixed pitch grating with 1.2 µm is used as a reference point, and 1.1/1.2 µm mixed pitch grating with 80, 60, 50, 40, and 20%, respectively, of 1.2 µm (8(1.2µm), 6(1.2µm), 5(1.2µm), 4(1.2µm), and 2(1.2µm) gratings) is investigated. Shifting from fixed pitch grating to mixed pitch 8(1.2µm) grating, the beam waisted increased from 26.4 to 28.6 µm due to undesired interaction between disproportionally mixed pitch. On the other hand, compared to 1.2 µm fixed pitch grating, 6(1.2µm), 5(1.2µm), and 4(1.2µm) mixed pitch gratings shows further reduction beam waist to 17.4 - 20 µm, with up to 34% of reduction. The obtained beam waist reduction can improve the accuracy of optical addressing on trapped $^{88}Sr+$ ion. On top of that, the developed Python-based data analysis techniques and codes can serve as a useful tool to automate the analysis of beam profiles at different heights for accurate optical addressing of ions under various trapping height, trapping conditions and ion trap designs.

5.2 Acknowledgments

This work was supported by ANR-NRF Joint Grant Call under Grant NRF2020-NRF-ANR073 HIT. We would also like to thank Advance Micro Foundry (AMF) for their support in multi-project wafer (MPW) fabrication.

5.3 Disclosures

The authors declare no conflicts of interest.

5.4 Data availability statement

Data underlying the results presented in this paper are not publicly available at this time but may be obtained from the authors upon reasonable request.

References

1. P. Zhao, Y. D. Lim, H. Y. Li, L. Guidoni, and C. S. Tan, "Advanced 3D Integration Technologies in Various Quantum Computing Devices," IEEE Open J. Nanotechnol. **2**(October), 1–1 (2021).
2. C. D. Bruzewicz, J. Chiaverini, R. McConnell, and J. M. Sage, "Trapped-ion quantum computing: Progress and challenges," Appl. Phys. Rev. **6**(2), (2019).
3. R. J. Niffenegger, J. Stuart, C. Sorace-Agaskar, D. Kharas, S. Bramhavar, C. D. Bruzewicz, W. Loh, R. T. Maxson, R. McConnell, D. Reens, G. N. West, J. M. Sage, and J. Chiaverini, "Integrated multi-wavelength control of an ion qubit," Nature **586**(7830), 538–542 (2020).
4. K. K. Mehta, "Integrated optical quantum manipulation and measurement of trapped ions," Massachusetts Institute of Technology (2017).
5. K. K. Mehta, C. Zhang, M. Malinowski, T. L. Nguyen, M. Stadler, and J. P. Home, "Integrated optical multi-ion quantum logic," Nature **586**(7830), 533–537 (2020).
6. K. K. Mehta, C. Zhang, M. Malinowski, T.-L. Nguyen, M. Stadler, and J. P. Home, "Integrated optical multi-ion quantum logic," (2020).
7. K. R. Brown, J. Kim, and C. Monroe, "Co-Designing a Scalable Quantum Computer with Trapped Atomic Ions," 1–11 (2016).
8. S. Li, L. Cai, D. Gao, J. Dong, J. Hou, C. Yang, S. Chen, and X. Zhang, "Deterministic design of focusing apodized subwavelength grating coupler based on weak form and transformation optics," Opt. Express **28**(23), 35395 (2020).
9. S. Kim, D. A. Westly, B. J. Roxworthy, Q. Li, A. Yulaev, K. Srinivasan, and V. A. Aksyuk, "Photonic waveguide to free-space Gaussian beam extreme mode converter," Light Sci. Appl. **7**(1), (2018).
10. H. Becker, C. J. Krückel, D. Van Thourhout, and M. J. R. Heck, "Out-of-plane focusing grating couplers for silicon photonics integration with optical mram technology," IEEE J. Sel. Top. Quantum Electron. **26**(2), 2–9 (2020).
11. Q. Zhong, V. Veerasubramanian, Y. Wang, W. Shi, D. Patel, S. Ghosh, A. Samani, L. Chrostowski, R. Bojko,

and D. V. Plant, "Focusing-curved subwavelength grating couplers for ultra-broadband silicon photonics optical interfaces," Opt. Express **22**(15), 18224 (2014).
12. G. T. Reed and A. P. Knights, *Silicon Photonics: An Introduction* (John Wiley & Sons, Ltd, 2004).
13. L. Cheng, S. Mao, Z. Li, Y. Han, and H. Y. Fu, "Grating couplers on silicon photonics: Design principles, emerging trends and practical issues," Micromachines **11**(7), (2020).
14. J. P. Likforman, V. Tugayé, S. Guibal, and L. Guidoni, "Precision measurement of the branching fractions of the 5p P1/2 2 state in Sr + 88 with a single ion in a microfabricated surface trap," Phys. Rev. A **93**(5), 1–9 (2016).
15. P. Dubé, A. A. Madej, Z. Zhou, and J. E. Bernard, "Evaluation of systematic shifts of the 88Sr+ single-ion optical frequency standard at the 10-17 level," Phys. Rev. A - At. Mol. Opt. Phys. **87**(2), 1–18 (2013).
16. Y. D. Lim, A. A. A. Apriyana, J. Tao, and C. S. Tan, "Ion Addressing Methodology By Laser Grating Coupler Via Ground-Slot Opening Of Ion-Traps," U.S. patent SG PRV 10201906375W (2019).
17. J. Tao, H. Y. Li, Y. D. Lim, P. Zhao, A. A. Alit Apriyana, L. Guidoni, and C. S. Tan, "Surface-Electrode Ion Trap with Ground Structures for Minimizing the Dielectric Loss in the Si Substrate," IEEE Trans. Components, Packag. Manuf. Technol. **10**(4), 679–685 (2020).
18. A. A. A. Apriyana, H. Li, P. Zhao, J. Tao, Y. Di. Lim, Y. Lin, L. Guidoni, and C. S. Tan, "Design and Development of Single-Qubit Ion Trap on Glass and Si Substrates with RF Analysis and Performance Benchmarking," IEEE Trans. Components, Packag. Manuf. Technol. **10**(7), 1221–1231 (2020).
19. P. Zhao, J. Tao, H. Y. Li, Y. D. Lim, L. Guidoni, and C. S. Tan, "Design, fabrication and characterization of surface electrode ion trap integrated with TSV," 2019 IEEE 21st Electron. Packag. Technol. Conf. EPTC 2019 13–17 (2019).
20. P. Zhao, J.-P. Likforman, H. Y. Li, J. Tao, T. Henner, Y. D. Lim, W. W. Seit, C. S. Tan, and L. Guidoni, "TSV-integrated Surface Electrode Ion Trap for Scalable Quantum Information Processing," Appl. Phys. Lett. **118**, 124003 (2021).
21. Y. D. Lim, "Python code to determine the angle of output light from gratings with different pitches," https://github.com/yd145763/mixed_pitch_grating_publication/blob/main/different pitch.py.
22. Y. D. Lim, "Python code to locate the peaks, and the corresponding beam waists and Gaussian plots in an E-field Plot," https://github.com/yd145763/mixed_pitch_grating_publication/blob/main/plot 2d along z direction.py.
23. Y. D. Lim, "Python code to determine the peaks, beam waists, mse to Gaussian fit, and max E-field at various heights (along z-axis)," https://github.com/yd145763/mixed_pitch_grating_publication/blob/main/find fwhm.py.
24. K. Li, K. Sasaki, K. Wake, T. Onishi, and S. Watanabe, "Quantitative Comparison of Power Densities Related to Electromagnetic Near-Field Exposures with Safety Guidelines from 6 to 100 GHz," IEEE Access **9**, 115801–115812 (2021).
25. Y. D. Lim, H. Y. Li, P. Zhao, J. Tao, L. Guidoni, and C. S. Tan, "Design and Fabrication of Grating Couplers for the Optical Addressing of Trapped Ions," IEEE Photonics J. **13**(4), 1–6 (2021).
26. D. Pascal, R. Orobtchouk, A. Layadi, A. Koster, and S. Laval, "Optimized coupling of a Gaussian beam into an optical waveguide with a grating coupler: comparison of experimental and theoretical results," Appl. Opt. **36**(12), 2443 (1997).
27. Y. D. Lim, "Python code to automatically locate the maximum point of a beam profile and plot x/y cut-off lines," https://github.com/yd145763/mixed_pitch_grating_publication/blob/main/max value column and rows no filtering.py.
28. Y. D. Lim, "Python code to determine the cut-off lines, FWHM, and Beam Waists along x- and y-axis of the beam," https://github.com/yd145763/mixed_pitch_grating_publication/blob/main/different mixture beam profiler and beam width plotting 4x mag.py.